Int J Earth Sci (Geol Rundsch) (2002) 91:964–978
DOI 10.1007/s00531-002-0280-0

ORIGINAL PAPER

François Guillot · Urs Schaltegger
Jean Michel Bertrand · Étienne Deloule
Thierry Baudin

Zircon U–Pb geochronology of Ordovician magmatism in the polycyclic Ruitor Massif (Internal W Alps)

Received: 9 July 2001 / Accepted: 2 March 2002 / Published online: 26 June 2002

Abstract Among the Middle Penninic basements of the Internal NW-Alps, the Ruitor massif shows the best preserved remnants of pre-Permian metamorphic rocks. Their Barrovian-type mineral associations are somewhat masked by the greenschist to blueschist Alpine metamorphism of Tertiary age. Four Ruitor gneisses have been analysed, showing geochemical characters of granitoids from orogenic zones. Zircon morphology also suggests magmatic protoliths and a crustal source; some of the morphological zircon types suggest anatectic granites. The first U–Pb ages on zircon for this massif have been obtained concurrently through conventional multigrain and ion microprobe dating. Two metavolcanic rocks at 471±5 and 468±22 Ma could be slightly older than the porphyritic augen gneisses at 465±11 and 460±7 Ma. Regional data from the other Internal basement massifs suggest that the Variscan event is poorly recorded, except in Ruitor-type units. Ruitor and Sapey gneisses belonged to the same unit (Nappe des Pontis), which was affected by a 480–450-Ma event including volcanism and anatexis and ended with a late calc-alkaline granite emplacement at 460–450 Ma. The distribution of Variscan basement units roughly parallels Alpine zonation.

Electronic supplementary material is available if you access this article at http://dx.doi.org/10.1007/s00531-002-0280-0. On that page (frame on the left side), a link takes you directly to the supplemenary material.

Keywords Internal Alps · Polycyclic metagranite · U–Pb geochronology · Variscan · Zircon morphology

Electronic supplementary material is available if you access this article at http://dx.doi.org/10.1007/s00531-002-0280-0. On that page (frame on the left side), a link takes you directly to the supplemenary material.

F. Guillot (✉)
UMR Processus et Bilans des Domaines Sédimentaires,
Univ. Sci. Tech. Lille bâtiment SN5,
59655 Villeneuve d'Ascq Cedex, France
e-mail: Francois.Guillot@univ-lille1.fr
Tel.: +33-320-542241

U. Schaltegger
Department of Earth Sciences,
Federal Institute of Technology ETH, 8092 Zürich, Switzerland

J.M. Bertrand
Laboratoire de Géodynamique des Chaînes Alpines,
Université de Savoie, 73376 Le-Bourget-du-Lac Cedex, France

É. Deloule
Centre de Recherches Pétrographiques et Géochimiques, BP 20,
54501 Vandoeuvre-lès-Nancy Cedex, France

T. Baudin
Bureau de Recherches Géologiques et Minières, BP 6009,
45060 Orléans Cedex, France

Present address:
U. Schaltegger, Département de Minéralogie,
Université de Genève, 13, rue des Maraîchers, 1205 Genève,
Switzerland

Introduction

The Ruitor Massif is one of the Briançonnais basement units that form the Italian and French southern equivalents of the Middle Penninic Grand-St-Bernard Nappe (GSB) in Switzerland. Several studies have dealt with the geology of the Ruitor Massif. They concern both its French part (Fabre 1961; Baudin 1987; Fabre et al. 1987) and its Italian to Swiss parts (Caby 1968; Burri 1983; Gouffon 1993; Cigolini 1995; Caby 1996; Gouffon and Burri 1997). The Ruitor Massif is in direct contact with the 'Zone Houillère Briançonnaise' (ZHB), the only continuous litho-structural unit of the Briançonnais domain from the Central Alps in Switzerland to the southern end of the Western Alps.

Cambrian to Ordovician ages were proposed in several recent papers for felsic magmatic components of the other Briançonnais basement units (Guillot et al. 1991; Bussy et al. 1996a, 1996b; Bertrand and Leterrier 1997; Bertrand et al. 1998, 2000a, 2000b). In most cases, the dated rocks represent a very small proportion of the bulk basement lithologies. All are retrograded to greenschist facies during the Alpine metamorphism. Ultramafic to mafic rocks have been dated by Stille and Tatsumoto

(1985) in the Berisal unit (Central Alps), suggesting Late Proterozoic komatiites as well as Ordovician to Cambrian tholeiitic-ultramafic components. The Ruitor massif belongs to the same Gd St Bernard zone as the Berisal unit. It was chosen as a target for two main reasons: (1) the Ruitor protoliths remained as the main undated piece of Middle Penninic basement; and (2) pre-Alpine metamorphic minerals are often well preserved so that our results should significantly constrain the age and number of the pre-Alpine magmatic and metamorphic events.

Conventional multi-grain methods of U–Pb dating on zircon are often hampered by poorly controlled effects of inheritance and radiogenic lead loss, especially in the case of metagranitoids of crustal origin. We had experienced such difficulties previously during the study of similar rocks, the Sapey gneisses (Bertrand et al. 1998; see their comparison with the Ruitor hereafter). Here we have cross checked two dating approaches that look well-adapted to such polymetamorphic rocks: high precision isotopic U–Pb dating on single zircon grains (IDTIMS) and in-situ zircon dating by ion microprobe (SIMS). Prior to the analytical work, a morphological study of the zircon populations was used to assess the magmatic character of the protoliths.

Geological setting

Because of its polycyclic character, the Ruitor Massif was considered as the basement of the monocyclic Zone Houillère Briançonnaise' (ZHB) by Fabre (1961) and Baudin (1987). The ZHB comprises an external, low-grade Upper Carboniferous formation (Briançonnais Coal Measures), which has yielded Namurian flora near the Petit St Bernard pass (Desmons and Mercier 1993) and tectonically overlies to the NW the oceanic Valais Zone (Fig. 1). The internal part of the ZHB is a thick, undated metaconglomerate wedge conventionally assumed of Stephanian age, metamorphosed under greenschist facies conditions. Marking the eastern, internal border of the ZHB along the metaconglomerate unit, the Ruitor gneisses and mica-schists grade southward to the narrower Sapey gneiss units (Détraz 1984; Bertrand et al. 1998) made of similar polycyclic rock-types. The Sapey gneisses are known to be capped by a thin metaconglomerate series of unknown age, representing an autochthonous sedimentary cover. The mylonitic contacts and the inverted position of the overlying ZHB sediments, however, preclude a basement-cover relationship with the ZHB (Bertrand et al. 1998). The nature of the western border of the Ruitor, at the contact with the ZHB, remains equivocal for similar reasons: first, the highly deformed metaconglomerates of possible Stephanian age are not dated; second, the geometrically lowest (Carboniferous?) sediments overlying the Ruitor basement locally show depositional criteria indicating an inverted, top-to-basement attitude (Mercier and Baudin 1990).

The Ruitor Massif is divided (Fig. 1) into two zones: (1) the External Ruitor where pre-Alpine mineralogical assemblages are relatively well preserved; they indicate a Barrovian-type (HT–MP) metamorphism (Gouffon 1993; Gouffon and Burri 1997) for which a Variscan age is well-documented (U–Pb on monazite: 330±2 Ma, Giorgis et al. 1999); and (2) the Internal Ruitor where Alpine overprint is dominant. The Internal Ruitor itself is divided into imbricates comprising Vanoise basement and Mesozoic, ocean-derived 'Schistes lustrés' units (section in Fig. 1 after Caby 1996). Internal and External Ruitor are locally separated by a slice of Permian–Triassic rocks, where Caby (1968, 1996) described an upside down depositional unconformity with the External Ruitor rocks.

The main contrast between the Ruitor–Sapey rocks and other basement units of the Briançonnais–Grand St Bernard domain consists in the presence of well-preserved relics of pre-Alpine metamorphic assemblages, which include biotite, muscovite, garnet, staurolite, kyanite, sillimanite and andalusite (Fabre 1961; Caby 1968; Bocquet [Desmons] 1974; Burri 1983; Baudin 1987, Gouffon 1993; Caby 1996; Gouffon and Burri 1997; Giorgis et al. 1999). Both Ruitor and Sapey gneisses are in tectonic contact to the east (Fig. 1) with the Vanoise basement together with Permian to Cainozoic sediments (Caby 1968; Guillot 1987; Guillot et al. 1993). By contrast, the Vanoise rocks contain preserved granophyre textures of Cambrian age (Guillot et al. 1991; Bertrand et al. 2000a), which suggest that pre-Alpine high-grade metamorphism was not recorded.

Lithology

Only External Ruitor rocks have been sampled for this study in order to avoid the ambiguous rock types of the Internal Ruitor, e.g. metasediments closely resembling flattened orthogneisses. According to Baudin (1987) and to Debelmas et al. (1991) several lithological groups may be defined in the External Ruitor. They are:

1. Mica-schists, where the dominant mineral associations are pre-Alpine garnet + muscovite, and/or staurolite, kyanite, chloritoid, andalusite; Alpine glaucophane + phengite + chlorite + albite.
2. Banded gneisses, which may be either quartz dominant, quartz + albite, two-mica gneisses or leucocratic gneisses.
3. Banded greenstones, locally associated with a marble horizon, which comprise an alternation of glaucophane-rich amphibolite, chlorite–albite green schist and leucocratic gneiss ('leptynite' of French authors, our samples ZH 98-18, 22). Garnet metapyroxenites may occur as boudins and stratabound amphibolites may be interleaved with metasediments as well as augen-bearing felsic rocks. As a whole, this is the typical 'leptyno-amphibolite' association described by French authors (see Discussion).
4. Augen gneisses and meta-pegmatites, which occur as relatively thin (up to 10 m) lens-shaped horizons parallel to the main foliation (see samples ZH 98-19, 20).

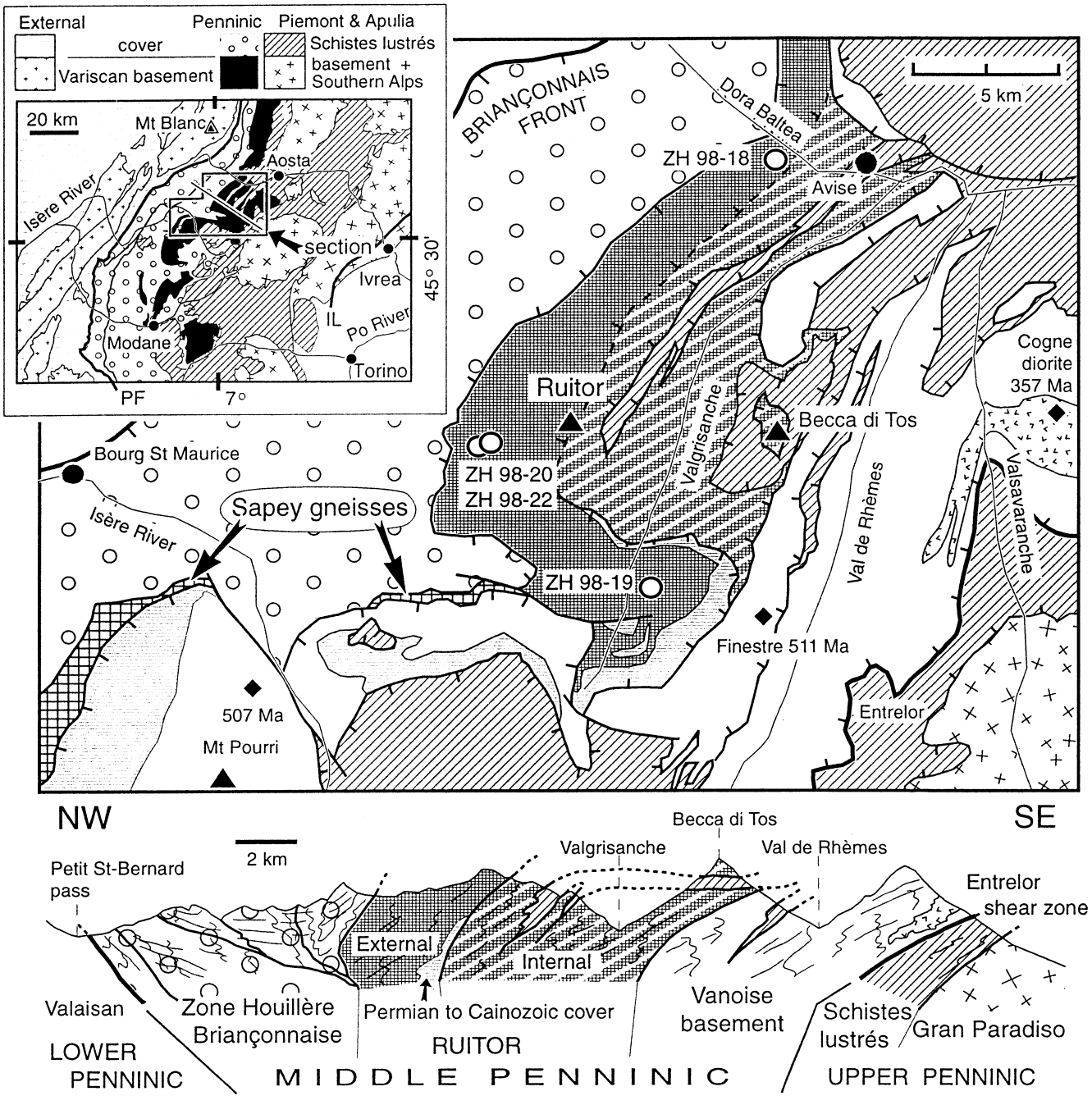

Fig. 1 Geological sketch map and cross section after Debelmas et al. (1991) with location of studied samples. *Full diamonds* with ages in Ma refer to Vanoise ages (Guillot et al. 1991; Bertrand et al. 2000a, 2000b). See unit names in the section (*bottom*) except Cogne diorite and Sapey gneisses, which are located on the map. *Insert* shows the situation of map and section; *PF* Penninic Front; *IL* Insubric Line

Assemblages (1) and (2) correspond to a metasedimentary sequence constituted by metapelites, impure sandstone and metagreywackes. Assemblages (3) and (4) correspond, respectively, to a dominantly tholeiitic metavolcanic origin (Eteradossi 1983; Stille and Tatsumoto 1985; Baudin 1987) and to anatectic intrusives (as suggested by zircon typology – see below).

Chemical composition and zircon morphology of analysed samples

The mineralogical description of the analysed samples is given in the Appendix. Because of the polymetamorphic character, field or thin section patterns do not help to determine unequivocally whether the rocks are meta-igneous or correspond to detrital horizons. The main criteria used in this study, therefore, are the chemical compositions of the samples (Table 1, Fig. 2) and the typology

Table 1 Geochemistry and age of dated samples (ZH 98-18 to -22) and of some Vanoise basements. All analyses have been performed by the Service d'Analyses, CRPG, Nancy from 1995 to 1999. Ages in the first four columns have been obtained from the present study whereas ages in the last six columns are from Bertrand et al. (2000a, 2000b)

Dated samples					Vanoise-zone felsic rocks					
Sample no.	ZH98-18	ZH98-19	ZH98-20	ZH98-22	96AM4	96AM6	ZH98-15	ZH98-16	ZH98-17	ZH95-18
Tect. unit, rock type	Ext. Ruitor, white gneiss	Ext. Ruitor, augen gneiss	Ext. Ruitor, augen gneiss	Ext. Ruitor, augen gneiss	Ambin, rhyolite	Ambin, rhyolite	Z. interna, grano-phyre	Z. interna, grano-phyre	Z. interna, grano-phyre	S. Vanoise, metagranite
Age (Ma)	468± 22 (2σ), IDTIMS	469± 15 (1σ), SIMS	460± 7 (2σ), IDTIMS	471± 2 (2σ), IDTIMS	500± 10 (1σ), SHRIMP		512± 7 (2σ), IDTIMS			479± 5 (2σ), IDTIMS
Major elements (%; *LOI* loss on ignition)										
SiO_2	73.81	68.29	73.19	70.07	72.74	74.69	75.67	75.14	75.99	74.87
Al_2O_3	13.77	16.15	13.60	14.91	12.70	13.05	12.92	12.91	12.59	12.20
Fe_2O_3 tot.	1.51	3.46	1.73	3.80	2.79	1.90	1.53	1.85	2.02	2.36
MnO	0.02	0.03	0.03	0.05	0.09	0.03	0.01	0.01	0.00	0.02
MgO	0.15	0.96	0.27	0.91	0.43	0.47	0.15	0.39	0.37	0.20
CaO	0.58	1.49	0.72	2.39	0.98	0.22	0.27	0.25	0.16	0.67
Na_2O	3.22	4.54	3.20	3.86	4.77	3.92	3.91	3.38	3.21	3.70
K_2O	4.82	2.51	4.73	2.53	3.06	3.71	4.98	5.32	4.70	4.31
TiO_2	0.07	0.46	0.12	0.30	0.24	0.28	0.16	0.16	0.15	0.24
P_2O_5	0.17	0.19	0.16	0.09	0.05	0.08	0.02	0.01	0.01	0.02
LOI	0.70	2.09	0.93	1.25	1.88	1.29	0.28	0.43	0.65	1.13
Total	98.82	100.17	98.68	100.16	99.73	99.64	99.90	99.85	99.85	99.72
Trace elements (ppm)										
Ba	158.6	616.2	156.9	560.1	528.0	468.0	499.0	532.0	469.4	827.0
Be	2.9	2.3	2.4	1.9	2.2	2.1	2.3	3.2	4.1	2.4
Co	0.8	5.7	1.5	5.4	0.8	1.9	0.7	0.8	0.9	1.4
Cr	2.7	21.4	10.2	13.4	2.3	2.7	7.9	2.5	3.4	7.5
Cu	4.4	8.7	5.7	5.1	7.8	10.8	3.8	8.2	8.6	5.6
Ga	20.4	22.4	19.7	19.1	21.4	21.0	23.0	23.8	22.9	24.0
Nb	10.7	12.2	9.5	6.0	15.0	14.0	14.7	14.4	14.5	11.4
Ni	1.8	9.9	3.8	7.8	1.4	11.7	2.6	1.5	1.9	2.6
Rb	221.0	88.4	240.0	89.7	93.7	104.9	169.9	199.3	161.0	140.3
Sr	61.0	123.1	52.7	161.4	102.0	38.8	18.6	25.2	18.8	39.2
Th	10.1	17.4	9.2	9.4	12.4	11.7	26.7	25.7	26.0	15.2
V	1.8	34.7	6.8	39.4	4.6	6.8	2.4	2.4	2.4	10.9
Y	25.4	35.2	23.3	20.5	73.3	52.2	81.4	78.1	78.4	71.1
Zn	17.0	52.2	32.8	60.4	16.7	23.9	32.9	63.4	32.4	63.0
Zr	67.5	195.0	77.4	135.8	412.0	415.0	286.8	285.3	291.1	365.0
Ge	1.03	1.14	1.40	0.82			0.98	1.05	0.77	1.67
As	0.55	0.63	0.48	0.25			0.31	0.55	0.67	1.36
Bi	0.22	0.04	0.02	0.01			0.31	0.88	0.28	0.07
Cd	0.09	0.05	0.17	0.15			0.08	0.16	0.21	
Cs	2.79	3.02	3.29	2.59			0.72	1.30	0.88	2.03
Hf	2.64	5.12	2.70	3.71			9.93	9.56	10.01	10.70
In	0.14	0.11	0.09	0.04			0.08	0.08	0.08	0.09
Mo	0.07	0.08	0.26	0.04			0.71	0.80	0.40	1.65
Pb	15.4	12.0	14.3	6.6			15.0	31.9	19.9	15.5
Sb	0.36	0.76	0.26	0.16			0.20	0.15	0.19	0.53
Sn	5.88	1.61	4.45	1.57			9.42	9.65	3.52	4.43
Ta	1.50	0.84	1.61	0.55			1.44	1.37	1.38	1.12
U	4.95	2.47	3.30	2.20			5.23	6.26	5.78	5.48
W	2.60	1.18	2.61	0.55			0.71	0.97	2.02	1.73
Rare earth elements (ppm)										
La	8.94	38.57	11.25	23.09	37.15	27.90	47.68	50.19	49.10	41.07
Ce	20.54	79.82	25.43	47.41	93.05	68.45	102.81	112.42	108.45	92.23
Pr	2.35	9.20	2.95	5.47	10.32	7.45	13.05	13.41	13.26	11.20
Nd	8.37	34.20	10.64	20.48	44.66	30.24	50.80	53.26	53.12	46.00
Sm	2.63	7.10	2.71	4.12	11.03	7.23	11.73	12.56	12.31	10.77
Eu	0.17	1.39	0.31	0.90	1.70	1.46	0.87	0.92	0.87	1.03
Gd	2.89	6.91	2.93	3.74	10.82	8.26	11.89	11.94	11.75	11.80
Tb	0.57	0.97	0.53	0.54	1.92	1.41	2.03	2.03	1.96	1.89
Dy	4.07	5.97	3.85	3.17	12.44	9.07	12.65	12.90	12.84	11.58

Table 1 (continued)

Dated samples					Vanoise-zone felsic rocks					
Sample no.	ZH98-18	ZH98-19	ZH98-20	ZH98-22	96AM4	96AM6	ZH98-15	ZH98-16	ZH98-17	ZH95-18
Tect. unit, rock type	Ext. Ruitor, white gneiss	Ext. Ruitor, augen gneiss	Ext. Ruitor, augen gneiss	Ext. Ruitor, augen gneiss	Ambin, rhyolite	Ambin, rhyolite	Z. interna, grano-phyre	Z. interna, grano-phyre	Z. interna, grano-phyre	S. Vanoise, metagranite
Age (Ma)	468± 22 (2σ), IDTIMS	469± 15 (1σ), SIMS	460± 7 (2σ), IDTIMS	471± 2 (2σ), IDTIMS	500± 10 (1σ), SHRIMP		512± 7 (2σ), IDTIMS			479± 5 (2σ), IDTIMS
Ho	0.82	1.24	0.75	0.69	2.77	2.02	2.72	2.73	2.68	2.55
Er	2.21	3.32	1.94	1.87	7.44	5.26	7.69	7.59	7.38	6.83
Tm	0.38	0.52	0.32	0.33	1.15	0.83	1.27	1.25	1.27	1.15
Yb	2.07	3.41	2.02	2.22	7.86	5.80	7.81	8.25	8.39	7.28
Lu	0.29	0.49	0.24	0.33	1.20	0.91	1.12	1.12	1.17	1.12
(La/Yb)*	2.9	7.6	3.8	7.0	3.2	3.2	4.1	4.1	4.0	3.8

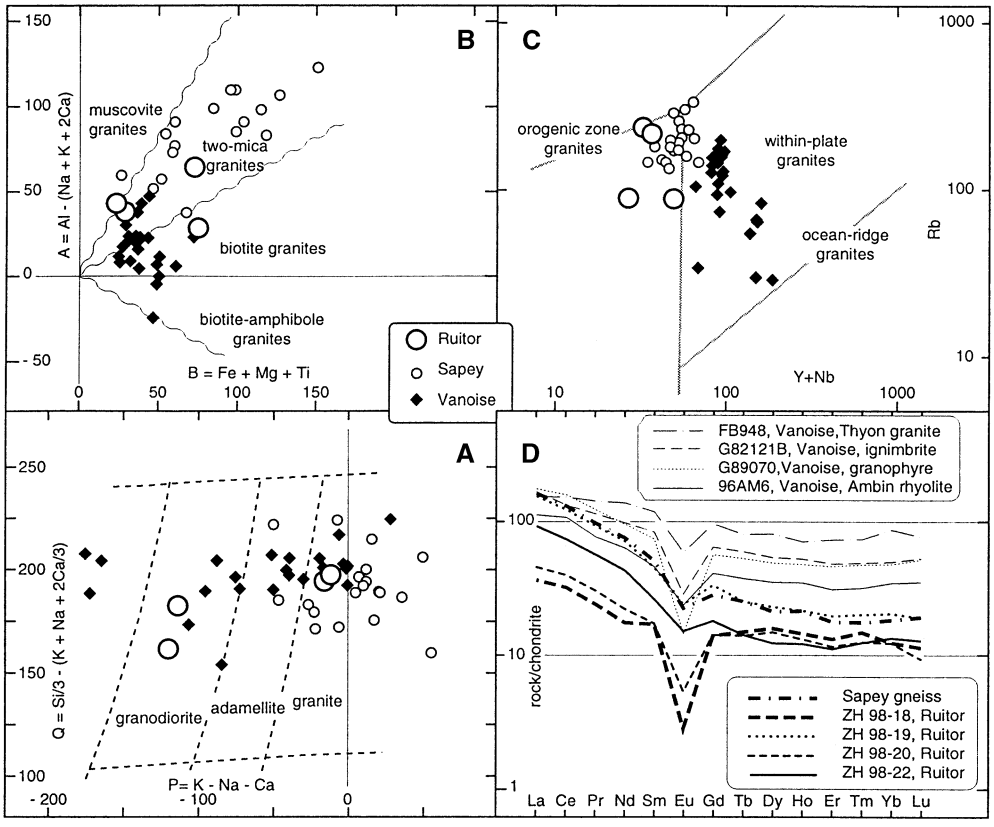

Fig. 2A–D Geochemistry of dated Ruitor rocks compared with Sapey gneisses and Vanoise basement felsics. New data (Table 1, eight analyses) and results from Saliot (1973, one analysis), Thélin (1983, 19 analyses), Guillot et al. (1993, nine analyses), Bussy et al. (1996a, six analyses), Bertrand et al. (1998, one analysis), Cosma (1999, one analysis), Beucler et al. (2000, seven analyses). **A, B** From Debon and Le Fort (1983, 1988; major elements in per cent of atom-gram per kg of rock). **C** Trace element plot (in ppm) with granite domains after Pearce et al. (1984). **D** Selected rare earth element profiles (ratios to chondrite composition after Evensen et al. (1978)

(as defined by Pupin 1980) of the separated zircon populations (Figs. 3 and 4). Two of the samples may correspond to a volcanic origin (ZH 98-18 and -22) whereas the others (ZH 98-19 and -20) may represent intrusive sills of anatectic granitoids.

Geochemistry

We have only listed (Table 1) previously unpublished data; a spreadsheet containing all the data used in the diagrams (Fig. 2) is available as electronic supplementary information. Our dated samples plot, together with most of the analyses taken for comparison, into the compositional field of granodiorite to granite (Fig. 2A). The balance between Al and the other major feldspar-constituent cations (Na, K, Ca) places the Sapey gneisses and the Ruitor samples on a peraluminous, calc-alkaline trend (muscovite granite and two-mica granite). By contrast, the Vanoise zone analyses plot mostly in the field of metaluminous-to-alkaline, mica-poor granites (Fig. 2B). Indeed, Vanoise rocks contain no muscovite and little

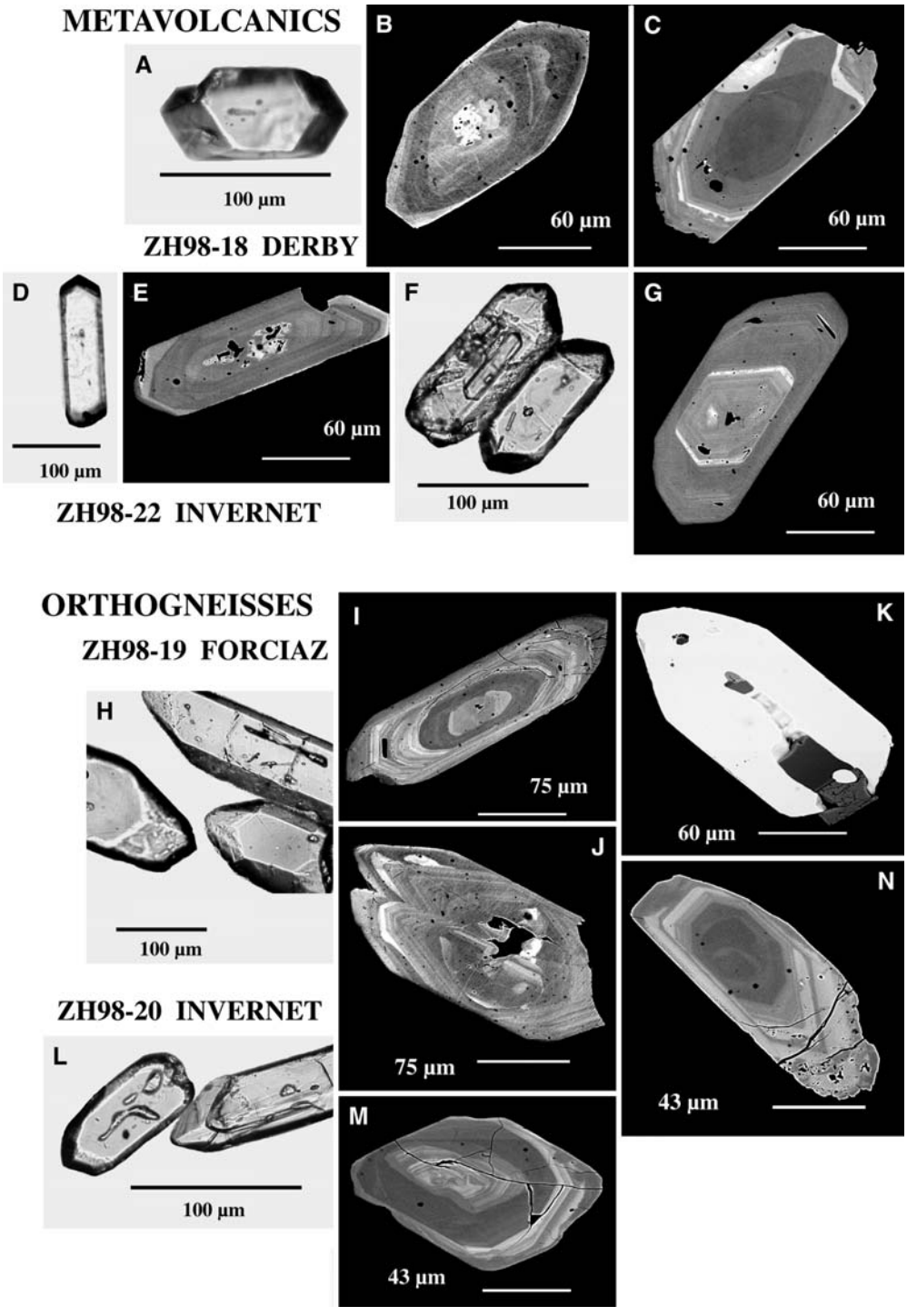

Fig. 3A–N Zircon images. Transmitted-light microscopy of whole crystals (**A**, **D**, **F**, **H**, **L**) and scanning electron microscopy in back-scattered electron mode (BSEM) of polished sections. The types hereafter are located in Fig. 4. Metavolcanics: ZH 98-18 Derby – **A** Homogeneous G-type zircon, small apatite inclusion. **B** Growth zoning with (white centre) U and Th concentration and quartz unmixing. **C** Dark inherited core unconformably surrounded by (*i*) a grey homogeneous rim (*ii*) a white rim and (*iii*) a zoned margin. ZH 98-22 Invernet – **D** G-type needle. **E** Quartz unmixing and U–Th concentration near the centre. **F** Inclusion-rich grains with (*top*) a possible negative crystal. **G** Homogeneous euhedral zoning – the inner part of the grain is not a core. Orthogneisses: ZH 98-19 Alpe La Forciaz – **H** S1–2 and S6–7 to S11–12-type zircons with major 211-pyramid and 110-prism. **I** Darker inherited core surrounded by growth zoning. **J** Cores and zoned imbricated crystals. **K** Polyphased magmatic inclusion (contrast has been enhanced) containing biotite, quartz and fluid(?). ZH 98-20 Invernet – **L** S16-type zircon (*left*) showing magmatic inclusion and S7-type (*right*) with a core. **M** Inherited core with, as in **C**, **I**, **J**, a grey homogeneous rim and a late, brighter zoned margin. **N** Dark core, euhedral zoning and late spongy overgrowth (late magmatic or metamorphic origin?)

green biotite (Guillot et al. 1993) whereas Ruitor and Sapey gneisses include both red biotite and muscovite of magmatic or metamorphic origin (Bertrand et al. 2000b, and this study). This difference is confirmed using the (Rb, Y + Nb)-plot (Fig. 2C), where the orogenic pattern of Sapey gneisses and Ruitor rocks (similar to S-type granites) contrasts with the anorogenic character of Vanoise felsic rocks (pertaining to A-type granites; Bussy et al. 1996a; Bertrand and Leterrier 1997; Beucler et al. 2000). Rare earth element (REE) data again evidence two groups (Fig. 2D): Vanoise felsic rocks have a flatter REE-profile [normalised-to-chondrite ratio: (La/Yb)*= 3.7, average of 21 analyses], with relatively more heavy REE than the Ruitor and Sapey rocks [(La/Yb)*=6.1, average of five analyses].

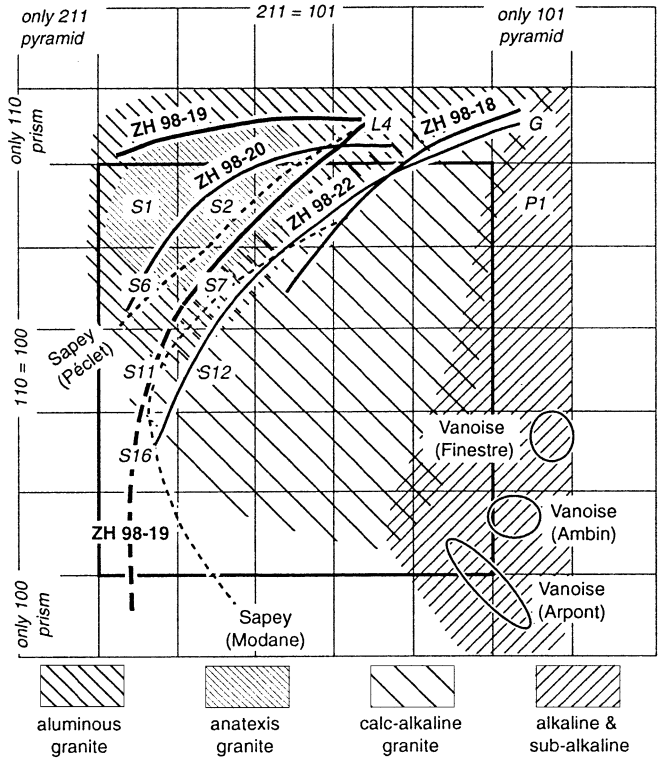

Fig. 4 Typological diagram of zircon morphology (Pupin 1980; main typological families as cross-hatched zones). Zircon types in italics (*L4*, *G*, *S1*...) refer to observed individual crystals (see Fig. 3 and text). For each of the Sapey and Ruitor samples, the distribution of types is indicated by a trend-line; the *upper right end of each trend line* corresponds to the location of types attributed to the end of magmatic crystallisation with lowest temperatures. Vanoise types fall into narrower fields (*ovals*)

Zircon typology

The prominence of euhedral zircon in all the analysed samples suggests a magmatic origin (Fig. 3). The presence of rounded grains in variable amounts does not preclude such an origin because the typology of the zircon populations confirms remelting of a crustal source. The zircon typology diagram (Fig. 4) was proposed by Pupin (1980) from a database of several hundred granitoids [pyramidal patterns – i.e. areal dominance either of (211)-pyramid or of (101)-pyramid – are plotted on the *x*-axis and are related to rock chemistry (respectively, peraluminous vs alkaline) whereas prismatic patterns – (110)-prism vs. (100)-prism – on the *y*-axis are related to crystallisation temperature (respectively,~500 vs. ~900 °C)]. We have compared the typology of the dated zircons with previously published data from the Briançonnais domain. All zircon populations from the analysed Ruitor samples and from previously analysed Sapey gneisses (Bertrand et al. 1998) are spread in the calc-alkaline to aluminous magmatic fields as defined by Pupin (1980). They contrast sharply with the metarhyolite, metagranophyre and metagranite of the Vanoise units (Guillot et al. 1991; Bussy et al. 1996a; Bertrand and Leterrier 1997; Cosma 1999; Bertrand et al. 2000a) whose zircon populations plot into the alkaline field.

Sample ZH 98-18

The zircon population consists of more than 60% of euhedral, colourless to pale pink grains. Among these grains a large part corresponds to G-P1 type zircons (101 pyramids only and dominant 110 prisms, Fig. 3A). According to Pupin (1980), such types represent the lowest temperature zircons, grown at the very end of magmatic crystallisation or related to metamorphism. The observed trend is close to the calc-alkaline trend defined by the same author (Fig. 4). Other grains are anhedral, brownish and non-transparent; they may represent xenocrysts (or scalped cores). The internal structure of the zircons (Fig. 3B, C), imaged by scanning electron microscopy in back-scattered electron mode (BSEM), shows that occasional cores are surrounded by zoned euhedral zircon and by a discontinuous light-coloured overgrowth. White zones may also occur either near the centre of grains (quartz–uranothorite-altered zircon association) or as a discontinuous ring following discontinuities (e.g. core-zoned domain); thorite, apatite and quartz inclusions are frequent.

Sample ZH 98-22

The zircon population is very similar to that of the ZH 98-18 sample, but richer in euhedral grains (Fig. 3D, F) and the spread of zircon types is greater (Fig. 4). Brown grains are full of tiny inclusions. The internal structure of the zircons imaged by BSEM shows scarce cores, often partly replaced by quartz and uranothorite, which are probably responsible for the turbid aspect of many grains (Fig. 3E, G).

Sample ZH 98-19

Zircons grains are pink in colour, most of them being euhedral, long and frequently needle-shaped with occasional occurrence of imbricated zoned crystals (Fig. 3J) suggesting a magmatic crystallisation. The dominant type (Pupin 1980) is S2-type (development of the 211 pyramid) and no G-type has been observed. Two separate trends converge to L4 types, the upper one (Fig. 4) corresponding to lower crystallisation temperatures after Pupin (1980). The mean population trend is closer to that of aluminous two-mica granites than to the calc-alkaline series. A small proportion of brown rounded grains is also present. The internal structure of the zircons imaged by BSEM shows a complex zoning with numerous cores (Fig. 3I, J). Fractures are healed by quartz, amphibole and monazite, the latter occurring also as rounded inclusions. Magmatic inclusions of biotite have also been observed (Fig. 3K). The rounded or irregular shape of

many grains is obviously not the result of a mechanical abrasion, but rather depends on specific crystallisation conditions (anatexis?).

Sample ZH 98-20

Zircons from this sample are pink to pale brown in colour and most of the grains are euhedral with S-type morphologies (Fig. 3L). Imbricated structures and large magmatic and fluid inclusions have been observed. However, rounded and darker grains are present in the zircon population. The typological trend-line of the zircon population falls into the anatectic granite field (Fig. 4). Internal structures imaged by BSEM show discordant cores surrounded by regularly zoned domains (Fig. 3M, N). Discontinuous overgrowths are anhedral to euhedral and show often a lace structure of quartz and zircon.

U–Pb geochronology

Analytical procedures

Two approaches were carried out simultaneously: (1) conventional isotope dilution and thermal ionisation mass spectrometry (IDTIMS) dating on small fractions (one to three zircon grains, total weight <13 μg) was performed at ETH Zürich, and (2) secondary ion mass spectrometry (SIMS) dating on polished zircon sections was carried out in CRPG Nancy using a Cameca IMS-1270 instrument. The selection of grains for either dating technique ensured homogeneous zircon morphologies were dated.

Conventional U–Pb dating

The zircons were extracted from the rock sample using standard techniques and the least magnetic fraction was collected on a Frantz magnetic separator. A further selection of inclusion- and crack-free zircons was abraded to remove marginal zones of lead loss. After cleaning in 4 *N* HNO_3 and thorough rinsing with water and acetone in an ultrasonic bath, the zircons were spiked with a mixed ^{205}Pb–^{235}U tracer solution and dissolved in HF–HNO_3. After chemical extraction, Pb and U were loaded with Si-Gel onto a Re filament, and the isotopic ratios of Pb^+ and UO_2 were analysed using an ion counting system mounted on a MAT 262 mass spectrometer. The performance of the ion counting system was monitored by repeated analyses of a NBS 982 standard solution. Total procedural blanks were estimated at 2±1 pg of Pb. Isotopic ratios and corresponding apparent ages are given in Table 2.

Ion microprobe dating

Selections of about 50 zircon grains from samples ZH 98-19 and ZH 98-20 were mounted on epoxy resin with a standard. The composition and age of the standard used in Nancy (zircon 91500) are described in Wiedenbeck et al. (1995). Optical microscope and scanning electron microscope (SEM) backscattered electron (BSE) imaging enabled a map to be drawn of the mounts that precisely determined the location of the spots to be analysed. After the runs, another SEM image was used to check the actual location and quality of the spots.

The O^{2-} primary ion beam was accelerated at 13 kV, with intensity ranging between 10 and 15 nA. The aperture illumination mode (Kohler illumination) was used with a 100-μm aperture to produce elliptical spots of 30 to 50 μm in diameter. Oxygen flooding was used to increase the O_2 pressure to 3.10^{-3} Pa (3.10^{-5} torr) in the sample chamber (Schuhmacher et al. 1994). Positive secondary ions were extracted with a 10 kV potential, and the spectrometer slits set for a mass resolution of~5,500 to separate isobaric interferences of HfSi from Pb. The field aperture was set to 6,000 μm, and the transfer optic magnification adjusted to 200. Rectangular lenses were activated in the secondary ion optic to increase the transmission at high mass resolution (de Chambost et al. 1996). The energy window was opened at 55 eV, with a 5 eV gap between the beginning of the energy distribution and the low energy side of the energy slit. Cleaning of the sample surface was done prior to analysis by rastering the primary beam over a 50×50 μm area. The masses $^{90}Zr_2{}^{16}O$, 203.5 (background), ^{204}Pb, ^{206}Pb, ^{207}Pb, ^{208}Pb, ^{238}U, $^{232}Th^{16}O$ and $^{238}U^{16}O$ were measured successively on a single collector used in ion-counting mode. Each analysis consisted of 15 successive cycles for 23 min. The mass and energy calibrations were checked before each measurement, and the 91500 standard zircon was measured every three sample analyses.

The reduction of data and common lead corrections were done using an Excel macro written by E. Deloule. An empirical linear relationship (Compston et al. 1984) was defined between UO^+/U^+ and Pb^+/U^+ from the set of standard measurements to define the relative sensitivity factor for Pb and U used for samples. A correction for common lead was made by measuring the ^{204}Pb amount and using the Stacey and Kramers (1975) model for terrestrial lead isotopic composition. The $^{206}Pb/^{204}Pb$ ratios ranged in most cases from 1,000 to more than 50,000, indicating that the common Pb composition chosen for correction was not highly critical.

Because of the size of the spots (40 μm), the precision of their location in the zircon grains was not very good and some of the spots may have comprised a combination of several zircon domains as defined from the BSEM imaging. Nevertheless, as more than half of the analyses were almost concordant, they should represent homogeneous domains within the zircon grains. Isotopic ratios and calculated ages are given in Table 3.

Table 2 Conventional IDTIMS U–Pb isotopic data. **Pb* Radiogenic Pb

No.	Aspect[a]	Weight (mg)	No. of grains	Concentrations				Atomic ratios						Apparent ages			Error corr.
				U (ppm)	*Pb (ppm)	Pb (pg)	Th/U[b]	$^{206}Pb/^{204}Pb$[c]	$^{206}*Pb/^{238}U$		$^{207}*Pb/^{235}U$		$^{207}Pb/^{206}Pb$		206/238	207/235	207/206	
									(d)	2σ (%)	(d)	2σ (%)	(d)	2σ (%)				
Metavolcanics																		
ZH 98-18, Derby, Aosta Valley																		
1	prism	0.0038	2	514	30.93	1.2	0.14	6,383	0.06366	0.36	0.4844	0.41	0.05518	0.21	397.9	401.1	419.6	0.86
2	prism	0.0037	2	386	26.81	89.0	0.21	91	0.07179	0.59	0.5553	4.90	0.05610	4.80	447.0	448.5	456.3	0.23
3	prism	0.0047	1	332	19.84	1.8	0.09	3,595	0.06420	0.34	0.4903	0.45	0.05538	0.22	401.2	405.1	427.5	0.88
4	prism incl	0.0025	1	353	23.64	0.9	0.15	4,373	0.07067	0.37	0.5449	0.44	0.05592	0.22	440.2	441.6	449.1	0.87
5	prism	0.0045	1	446	26.27	1.0	0.11	7,818	0.06286	0.35	0.4765	0.41	0.05498	0.18	393.0	395.7	411.3	0.90
6	spr S	0.0129	2	513	30.73	3.3	0.14	8,063	0.06332	0.34	0.4817	0.39	0.05518	0.13	395.8	399.3	419.6	0.95
ZH 98-22, Glacier de l'Invernet																		
7	prism p	0.0066	3	533	39.90	82.4	0.33	221	0.07497	0.37	0.5819	1.50	0.05629	1.44	466.1	465.7	463.9	0.28
8	lpr incl	0.0066	3	376	29.50	5.9	0.50	2,028	0.07488	0.33	0.5825	0.43	0.05342	0.21	465.5	466.1	468.9	0.88
9	prism	0.0065	2	477	35.81	1.7	0.34	8,513	0.07501	0.34	0.5843	0.40	0.05650	0.15	466.3	467.3	472.2	0.93
10	Platy P	0.0050	1	659	47.72	6.4	0.32	2,382	0.07248	0.35	0.5792	0.41	0.05796	0.21	451.1	464.0	528.4	0.86
11	prism incl.	0.0039	3	469	34.38	21.6	0.24	421	0.07505	0.35	0.6025	0.82	0.05823	0.71	466.5	478.8	538.4	0.51
12	spr incl	0.0054	2	500	36.22	3.0	0.27	4,174	0.07367	0.39	0.5738	0.44	0.05650	0.22	458.2	460.5	471.9	0.87
Porphyritic orthogneiss																		
ZH 98-20, Glacier de l'Invernet																		
13	prism	0.0068	1	437	29.57	2.2	0.10	6,352	0.07228	0.34	0.5584	0.40	0.05603	0.16	449.9	450.5	453.7	0.92
14	lpr P br	0.0035	3	345	23.26	2.2	0.09	2,547	0.07225	0.36	0.5591	0.48	0.05613	0.29	449.7	451.0	457.4	0.80
15	spr S	0.0057	1	435	25.37	5.4	0.10	1,828	0.06245	0.35	0.4748	0.44	0.05514	0.25	390.5	394.5	418.0	0.82
16	lpr P	0.0046	1	219	14.47	6.1	0.11	754	0.07031	0.37	0.5431	0.65	0.05602	0.49	438.0	440.5	453.1	0.66
17	prism	0.0089	2	384	26.86	6.7	0.11	2,434	0.07464	0.34	0.5871	0.42	0.05705	0.19	464.2	469.0	493.0	0.90

[a] *br* Brownish; *incl* inclusions; *lpr* long prismatic; *prism* prismatic; *spr* short prismatic; *P, S* morphological types (Pupin 1980)

[b] Calculated on the basis of radiogenic $^{208}Pb/^{206}Pb$ ratios, assuming concordancy

[c] Corrected for fractionation and spike

[d] Corrected for fractionation, spike, blank and common lead (Stacey and Kramers 1975)

Table 3 SIMS U–Pb isotopic data. *T* Zoned tips; *C* centres; *R* includes epoxy mount; *f* ill-focussed spot; + well-located on tip or centre; – includes several domains; ±1-σ error

Spot	Type	206/204	Pb (ppm)	U (ppm)	Th (ppm)	$^{207}Pb/^{235}U$ (±%)	$^{206}Pb/^{238}U$ (±%)	Correl.	Age 207/235 (Ma)	Age 206/238 (Ma)	Age 207/206 (Ma)
Sample ZH 98-19, Alpe La Forciaz orthogneiss											
19-1	C+R	58,278	64	584	154	1.153±1.9	0.1281±2.0	0.99	779±11	777±15	784±7
19-2	T+	130,269	59	590	60	1.012±2.1	0.1166±2.1	0.99	710±11	711±14	707±7
19-4	T+R	6,178	20	297	40	0.616±2.1	0.0783±2.0	0.98	487±8	486±10	494±10
19-8	C–R	100,463	87	673	422	1.447±2.0	0.1508±2.0	1	909±12	906±17	916±4
19-10	T–R	13,841	8	126	80	0.613±2.1	0.0771±2.1	0.95	485±8	479±10	518±13
19-11	T–R	48,137	16	246	47	0.541±2.0	0.0730±1.9	0.96	439±7	454±9	362±13
19-15	T–R	22,452	18	289	48	0.582±2.1	0.0730±2.1	0.98	466±8	454±9	524±7
19-16c	C+	34,482	21	379	30	0.512±2.1	0.0648±2.0	0.98	419±7	405±8	503±9
19-16t	T–R	5,190	26	614	56	0.394±2.3	0.0500±2.0	0.93	337±6	314±6	496±16
19-17	T–R	2,767	12	209	35	0.516±2.9	0.0651±2.1	0.73	422±10	406±8	510±40
19-18	C–R	14,784	11	211	20	0.487±2.1	0.0625±1.9	0.99	403±7	391±7	473±7
19-23	T–R	111,040	79	1142	109	0.630±2.1	0.0808±2.0	1	496±8	501±10	476±4
19-27	T–R	8,131	15	225	30	0.599±2.3	0.0767±2.2	0.93	476±9	476±10	476±17
19-28	C+	11,090	78	1344	409	0.564±1.9	0.0671±1.9	1	454±7	419±8	637±4
19-29	C+	51,509	25	391	37	0.575±1.9	0.0734±1.9	0.99	461±7	457±9	484±6
19-40	Tf	33,811	27	402	47	0.594±2.0	0.0772±1.9	0.99	473±8	480±9	444±7
19-45	Tf	44,024	21	328	53	0.578±1.9	0.0745±2.0	0.99	463±7	463±9	464±4
Sample ZH 98-20, Invernet orthogneiss											
20-6	Cf	84,897	42	294	100	2.300±2.2	0.1646±2.2	0.98	1,212±16	982±20	1,648±8
20-8	Tf	83,285	73	1544	154	0.422±1.9	0.0547±2.0	1	357±6	343±7	450±4
20-9	Tf	24,396	20	327	63	0.560±2.0	0.0715±2.0	1	451±7	445±9	482±3
20-10	Tf	8,759	58	424	125	1.218±2.5	0.1604±2.3	0.93	809±14	959±20	415±18
20-11	Tf	24,898	31	519	53	0.550±2.0	0.0696±2.0	0.99	445±7	433±8	505±6
20-15	Tf	20,115	19	272	38	0.629±2.1	0.0803±2.0	0.99	496±8	498±10	485±6
20-17	Tf	81,037	49	673	45	0.754±4.4	0.0842±2.7	0.61	570±19	521±13	771±74

Geochronological results

Metavolcanics

ZH 98-18

Six fractions of one to two grains were analysed by ID-TIMS (Fig. 5A, Table 2). Except for point (6), only G-P1 types were analysed. Analytical points were discordant and were only poorly aligned along the discordia. The most concordant point (2) had a large contribution of common Pb, which resulted in a large error on the calculated age. Isoplot calculation (Ludwig 1999) yields an upper intercept age of 468±22 Ma (MSWD=2.8) and a lower intercept at 284±51 Ma.

ZH 98-22

Six fractions of one to three grains were analysed by ID-TIMS (Fig. 5B). Except for point (12), only G or P1 types were analysed. Analytical points are scattered, but three of them are almost concordant. Two points (10 and 11) are far from the concordia and correspond probably to inheritance possibly coupled to lead loss. An isoplot calculation excluding these points and the bad analysis (7) yields an age of 471±5 Ma (MSWD=1.13) with a lower intercept close to zero.

Porphyritic orthogneisses

ZH 98-19

Seventeen analyses were obtained by SIMS (Fig. 6, Table 3). Apparent $^{206}Pb/^{238}U$ ages are scattered from 314 to 906 Ma with a main grouping around 400–500 Ma. Three points (1, 2, 8, not represented in Fig. 6), which are almost concordant at ca. 910, 780 and 710 Ma, obviously represent inherited parts of zircon whereas one outlier point (16 t, not shown) at 314 Ma, with a $^{207}Pb/^{206}Pb$ age near 496 Ma, probably endured a pronounced lead loss. The subconcordant ellipses (Fig. 6A) located close to the 480 Ma group (eight points: 4, 10, 15, 23, 27, 29, 40, 45) yield an imprecise upper intercept age at 487±40 Ma. Among 13 spots with apparent ages ranging from 400 to 500 Ma (Fig. 6B), the 454–480-Ma group of $^{206}Pb/^{238}U$ ages with seven points gives a weighted average of 465±11 Ma at 95% confidence (14% probability of fit, using the 'WtdAv' function from the Isoplot program; Ludwig 1999).

ZH 98-20

Five fractions consisting of one to three grains were analysed by IDTIMS (Fig. 5C). The analytical points are well-aligned, rejecting fraction (17) with probable inher-

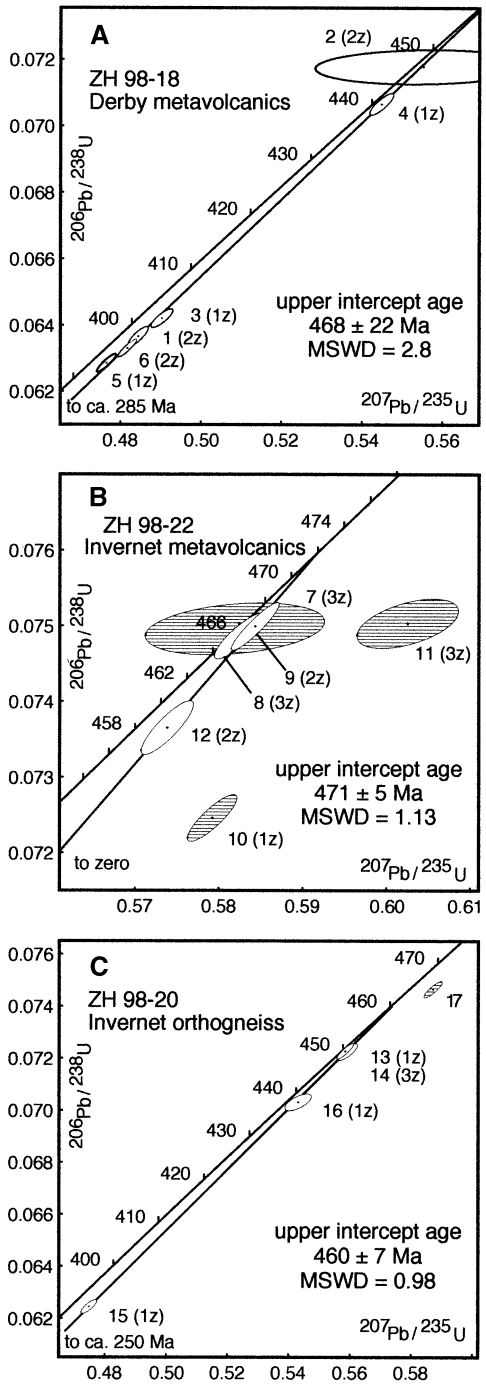

Fig. 5A–C U–Pb concordia diagrams: **A** for metavolcanic gneiss ZH 98-18, **B** for metavolcanic gneiss ZH 98-22, **C** for leucocratic orthogneiss ZH 98-20. Each zircon fraction 1–17 (Table 2) is indicated with its number of grains in parentheses. Data for cross-hatched ellipses have been discarded from the age calculation

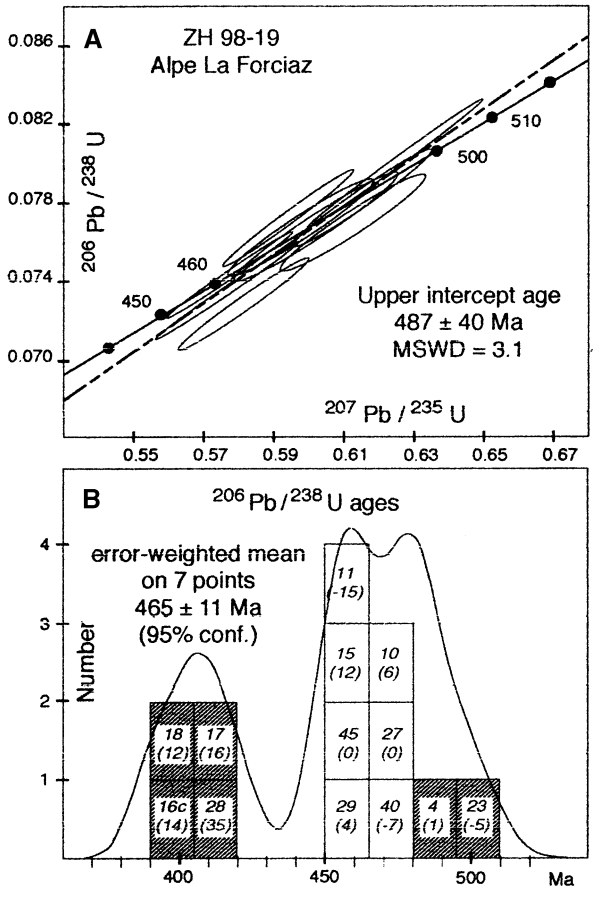

Fig. 6A, B Ion probe data for augen gneiss ZH 98-19. **A** Error ellipses and discordia line of the eight near-concordant points around 480 Ma. **B** Distribution of the 13 $^{206}Pb/^{238}U$ ages between 391 and 501 Ma; cross-hatched box data have not been used to compute the mean. The *figures in each box* are the spot number and, within parentheses, the difference in Ma between the $^{207}Pb/^{235}U$ apparent age and the $^{206}Pb/^{238}U$ apparent age (Table 3)

itance. They yield an upper intercept age of 460±7 Ma (MSWD=0.98) and a lower intercept at 248±37 Ma. The upper intercept age is interpreted as the age of the granite emplacement.

An attempt at SIMS dating was made for this sample. Unfortunately, the seven analysed spots display a large scatter with no significant grouping. Four are poorly aligned and yield an upper intercept age at 504±60 Ma (MSWD=90). A near concordant point (15) corresponds to a $^{207}Pb/^{206}Pb$ age of 485±6 Ma, this latter age being far from the error margin calculated on the same sample by the conventional method on single zircons.

Discussion and conclusions

The petrology and the geochemistry of the various Ruitor rock types have not yet been investigated in detail. Thus, the presumed magmatic origin of the dated felsic rocks was assessed. From this respect, the geochemical data, in fair agreement with the zircon typology, are in favour of magmatic products derived from calc-alkaline magmatism.

An Ordovician history is clearly demonstrated. The upper intercepts from ZH 98-22 (471±5 Ma, metavolcanics) and ZH 98-20 (460±7 Ma, orthogneiss) stand out as the best age data, whereas the other less precise results

are still consistent with Ordovician events. The conventional IDTIMS Ruitor ages are spread between 471 and 460 Ma. A tentative ion probe upper intercept age of sample ZH 98-19 appears older with a larger error at 487±40 Ma, but the more probable mean age of 465±11 Ma obtained from the distribution of $^{206}Pb/^{238}U$ ages is interpreted as the age of the protolith. It is similar to IDTIMS ages of the other samples. Thus, IDTIMS and SIMS errors overlap. A direct comparison attempted with sample ZH 98-20 was inconclusive because of the poor quality of the SIMS results obtained on this sample. Similarly, our SIMS data could be taken to imply a protracted zircon crystallisation history in the lower Palaeozoic, but large and chaotic variations among the three calculated ages (Table 3) are rather to be related to underestimated zircon complications.

Regarding the Ruitor history, all our results are within errors and it is only possible to propose a tentative sequence of events. Our older Ruitor ages correspond to metavolcanics. Sample ZH 98-18 (468±22 Ma) belongs to a layered bimodal association of 'leptyno-amphibolite', which is likely to represent a metamorphosed volcanic suite. Its age should date the primary emplacement of (part of) the Ruitor body. Sample ZH 98-22 has the best-constrained age (471±5 Ma) and probably represents a similar primary emplacement. Because the K-feldspar megacryst-bearing orthogneisses may be younger (ZH 98-19 at 465±11 Ma and ZH 98-20 at 460±7 Ma), they might correspond to subsequent granitoid intrusions. A confirmation of this relative chronology might be found in the field by verifying the intrusive character of the K-feldspar orthogneiss protolith, but the only clue we are aware of is a pegmatite body quoted by Caby (1996).

For the age of metamorphism, an indication is given by the lower intercept ages of two samples (ZH 98-18 and ZH 98-20), which suggest lead loss during some Variscan overprint. A Variscan high temperature (HT)-event was clearly demonstrated in the Mont Mort area (Bussy et al. 1996b; Giorgis et al. 1999), which belongs to a northern extension of the Ruitor Massif. Until now, the Ruitor (including Mont Mort) units are the only internal basement units of Western Alps where a Variscan metamorphic signature has been found. In other Penninic and Piemont units, orthogneisses are either too old (Cogne granodiorite at 360 Ma – Bertrand et al. 2000b) or clearly late to post-Variscan (Permian ages in Gran Paradiso and Dora Maira; Bussy and Cadoppi 1996; Bertrand et al. 2000b).

On the basis of their proximity with the ZHB and of the good preservation of pre-Alpine relics, the Ruitor and Sapey units were recently grouped in a single Alpine nappe, the 'Nappe des Pontis' (Gouffon 1993; Gouffon and Burri 1997). We may now add three other strong similarities: (1) the ages obtained on orthogneisses, (2) the typology of the zircon population and (3) the whole-rock geochemistry.

A clear difference is established between the Vanoise and Ruitor–Sapey orthogneisses. Ruitor and Sapey granitoids are of crustal origin, and were probably generated in a common pre-Variscan orogenic setting of 450–480 Ma age. By contrast, the 480–520 Ma-old alkaline metarhyolites and metagranites from the Vanoise, Ambin and Siviez–Mischabel basement units belong to earlier, anorogenic geodynamic settings. There the Variscan event is hardly detectable, and so the difference has apparently lasted until Late Palaeozoic times. To account for the variation in Variscan influences, Platt et al. (1989, p. 136) proposed that the Ruitor units were at a deeper pre-Alpine crustal level than the Vanoise basement units. The similarity between their unconformable Permian–Triassic covers suggests a relative proximity at the end of Variscan times.

Concerning the methods, the zircon typology of Pupin (1980) appears to be a robust indicator of magmatic processes. This method has helped us to demonstrate anatexis, putting a stronger constraint on the tectonic setting of the granitoid protoliths. The zircon typology determination is inexpensive and easy to perform; therefore, we suggest zircon typology should be incorporated as a standard method in the zircon-dating procedure.

In the Ordovician, what occurred in and between the pre-Variscan portions of Europe is still an open question, despite numerous recently published geochronological data (e.g. Valverde-Vaquero and Dunning 2000, and references therein) and a wealth of tentative palaeogeographical reconstructions (Ziegler 1990; Pin and Marini 1993; von Raumer 1998). The Alps, and especially their internal domains, are obviously not the best place for precise reconstructions because of all the displacements and/or rotations that occurred during the Variscan and Alpine orogenies. What we need, initially, is a robust chronology and some indication of the palaeotectonic setting of the dated magmatic rocks. Do all Ordovician-dated rocks represent extensional settings, as it has often been proposed for 'leptyno-amphibolite' bimodal metavolcanics (Paquette et al. 1989; Pin and Marini 1993 and references therein), or did a collision-related process produce Ordovician eclogites or migmatites (Schaltegger and Gebauer 1999)? Our study of the Ruitor area only demonstrates that an important part of the Ruitor complex was formed during Ordovician times in an orogenic setting, but many unsolved questions remain. Ruitor eclogite occurrences, still poorly studied, are difficult to relate to the Variscan HT-event and could indicate, instead, a high-pressure episode of Alpine or pre-Alpine age. Desmons and Mercier (1993) have proposed the polycyclic Ruitor Massif to be older than the 500-Ma monocyclic Vanoise. We have found, instead, younger ages in the Ruitor felsics, but we cannot exclude older, e.g. Pan-African-age rocks, to be also present. Indeed, most magmatic remnants in the Alpine-reworked basements occur as small disseminated bodies within large meta-sedimentary assemblages of poorly known age.

To conclude, three distinctive belts may be defined from west to east within the Pennine–Piemont domain of the Western Alps (Fig. 7):

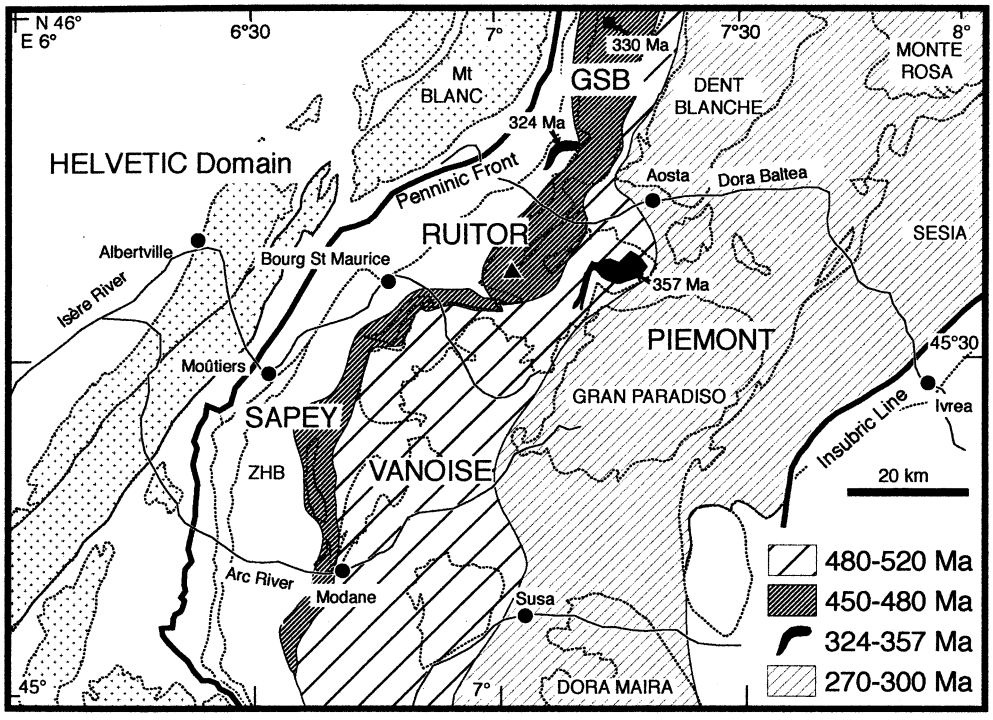

Fig. 7 Variscan domains in the Penninic Alps. The exposed basement massifs are outlined by *dotted lines*

1. Ruitor–Sapey (Nappe des Pontis in Switzerland) characterised by ca. 480–450 Ma-old aluminous intrusives and Variscan high-grade metamorphism around 330 Ma (Giorgis et al. 1999);
2. Vanoise (Mont Fallère and Siviez-Mischabel in Switzerland) characterised by 520–480 Ma-old alkaline magmatism and few (observed) traces of Variscan metamorphism;
3. Gran Paradiso, Dora Maira and Monte Rosa, where dating is still in progress with Ordovician orthogneisses (Bussy and Cadoppi 1996) and a large amount of Late Carboniferous to Permian intrusives (Bussy and Cadoppi 1996; Bertrand et al. 2000b; von Raumer et al. 2002).

These three belts probably correspond to distinctive Variscan terranes within the Hun Super-Terrane defined along the continental margin of Gondwana (Stampfli 1990, 1996). Because this Super-Terrane perhaps contains island arcs as well as passive continental margins (see a more up-to-date reconstruction in von Raumer et al. 2002), the rock record preserved today may well represent very contrasting geodynamic settings. This Variscan contrast is further enhanced by distinctive behaviours during post-Variscan extension, and during the Alpine subduction and exhumation stages.

Acknowledgements This paper results from a joint project between France (Chambéry University) and Switzerland (ETH Zürich) and was funded by the French Embassy in Bern and by the GeoFrance3D program (MENRT, INSU, BRGM). Use of the Cameca IMS 1270 ion probe was supported by the INSU-CNRS national instrument program. Jacques Leterrier and Jérôme Ganne are thanked for their help during sampling. The careful reviews of J. von Raumer and M.H. Dodson greatly improved the paper.

Appendix

Sample descriptions

Sample ZH 98-18

Sample ZH 98-18 is a leucocratic gneiss interlayered with amphibolites, sampled near the village of Derby (Aosta Valley, Italy – N45°43.0′, E7°06.6′, 790 m). It belongs to the banded greenstone group defined by Baudin (1987). It contains small fractured clasts of microcline, which occurs also in the groundmass with quartz and albite. The dominant mica is a fine-grained alpine phengite, but larger white micas, slightly oblique on the foliation, may be older. Accessory minerals are large apatites, zircon and allanite replaced by retrograde epidote and clinozoisite.

Sample ZH 98-19

Sample ZH 98-19 is a mesocratic K-feldspar megacryst-bearing augen gneiss sampled at Alpe du Mont Forciaz, near Usellières in Valgrisanche (Aosta Valley, Italy – N45°35.0′, E7°02.8′, 2,180 m). It comprises mostly large K-feldspar partly replaced by chessboard albite, quartz and some secondary calcite. The rock contains also phengite, chlorite and stilpnomelane. Accessories are apatite, titanite and zircon.

Sample ZH 98-20

Sample ZH 98-20 is a leucocratic K-feldspar megacryst-bearing augen gneiss sampled in a scree below an exposure located on the southern side of the Glacier de l'Invernet (Ste-Foy-Tarentaise, Savoy, France – N45°37.05′, E6°59.0′, ~2,650 m). It comprises numerous megacrysts of perthitic K-feldspar, quartz, albite and epidote. Small broken garnets are associated with epidote. Accessories are apatite, titanite and zircon.

Sample ZH 98-22

Sample ZH 98-22 is a dark fine-grained gneiss (‘métakératophyres oeillés’ in Baudin 1987) sampled in a boulder of the north lateral moraine of the Glacier de l’Invernet (same location as ZH 98-20). Small augen correspond to quartz and albite. It comprises phengite, pale brown biotite, occasional blue-green actinolite, small garnets, with abundant epidote and minor titanite and zircon.

References

Baudin T (1987) Étude géologique du massif du Ruitor (Alpes franco-italiennes): évolution structurale d’un socle briançonnais. PhD Thesis, University of Grenoble

Bertrand JM, Leterrier J (1997) Early Paleozoic granitoids in the southern Vanoise basement: U–Pb geochronology of the Arpont metagranite (Savoy, French Alps) (English abridged version). CR Acad Sci IIA 325:839–844

Bertrand JM, Guillot F, Leterrier J, Perruchot MP, Aillères L, Macaudière J (1998) Granitoïdes de la zone houillère briançonnaise en Savoie et en Val d’Aoste (Alpes occidentales): géologie et géochronologie U–Pb sur zircon. Geodin Acta 11:33–49

Bertrand JM, Guillot F, Leterrier J (2000a) Early Paleozoic U–Pb age of zircons from metagranophyres of the Grand-Saint-Bernard Nappe (zona interna, Aosta Valley, Italy) (English abridged version). CR Acad Sci IIA 330:473–478

Bertrand JM, Pidgeon RT, Leterrier J, Guillot F, Gasquet D, Gattiglio M (2000b) SHRIMP and IDTIMS U–Pb zircon ages of the pre-Alpine basement in the Internal Western Alps (Savoy and Piedmont). Schweiz Mineral Petrogr Mitt 80:225–248

Beucler M, Guillot F, Hernandez J (2000) Les granophyres du Mont Pourri (Vanoise septentrionale – Savoie): lithostratigraphie et pétrologie. Bull Soc Vaud Sci Nat 87:29–60

Bocquet (Desmons) J (1974) Études minéralogiques et pétrologiques sur les métamorphismes d’âge alpin dans les Alpes françaises. Thèse État, University of Grenoble

Burri M (1983) Description géologique du front du St-Bernard dans les vallées de Bagnes et d’Entremont (Valais). Bull Lab Géol, Univ Lausanne

Bussy F, Cadoppi P (1996) U–Pb zircon dating of granitoids from the Dora-Maira massif (western Italian Alps). Schweiz Mineral Petrogr Mitt 76:217–233

Bussy F, Derron MH, Jacquod J, Sartori M, Thélin P (1996a) The 500 Ma-old Thyon metagranite: a new A-type granite occurrence in the Penninic realm (Western Alps, Wallis, Switzerland). Eur J Mineral 8:565–575

Bussy F, Sartori M, Thélin P (1996b) U–Pb zircon dating in the middle Penninic basement of the Western Alps (Valais, Switzerland). Schweiz Mineral Petrogr Mitt 76:81–84

Caby R (1968) Contribution à l’étude structurale des Alpes Occidentales: subdivisions stratigraphiques et structure de la zone du Grand-Saint-Bernard dans la partie sud du Val d’Aoste (Italie). Trav Lab Géol Fac Sci Grenoble 44:95–111

Caby R (1996) Low-angle extrusion of high-pressure rocks and the balance between outward and inward displacements of Middle Penninic units in the Western Alps. Eclog Geol Helv 89:229–267

Cigolini C (1995) Geology of the Internal Zone of the Grand Saint Bernard Nappe: a metamorphic Late Paleozoic volcano-sedimentary sequence in south-western Aosta Valley (Western Alps). In: Lombardo B (ed) Studies on metamorphic rocks and minerals of the Western Alps, Boll Mus Reg Sci Nat 13(suppl):293–328

Compston W, Williams IS, Meyer C (1984) U–Pb geochronology of zircons from lunar breccia 73217 using a sensitive high mass-resolution ion microprobe. J Geophys Res 89(Suppl): B525–534

Cosma L (1999) Géologie et magmatisme paléozoïque en Vanoise septentrionale (La Sauvire, Plan Richard), implications géodynamiques. Dipl Géol Minéral, University of Lausanne

de Chambost E, Schuhmacher M, Lovestam G, Claesson S (1996) Achieving high transmission with the Cameca IMS-1270. In: Benninghoven A et al. (eds) Secondary ion mass spectrometry, SIMS X. Wiley, New York, pp 1003–1006

Debelmas J, Caby R, Antoine P, Elter G, Elter P, Govi M, Fabre J, Baudin T, Marion R, Jaillard É, Mercier D, Guillot F (1991) Feuille Sainte-Foy-Tarentaise. Carte Géol France, 1/50,000, 728 (map and notice)

Debon F, Le Fort P (1983) A chemical–mineralogical classification of common plutonic rocks and associations. Trans R Soc Edinb Earth Sci 73:135–149

Debon F, Le Fort P (1988) A cationic classification of common plutonic rocks and their magmatic associations: principles, method, applications. Bull Minéral 3:493–510

Desmons J, Mercier D (1993) Passing through the Briançon Zone. In: von Raumer JF, Neubauer F (eds) The pre-Mesozoic geology in the Alps. Springer, Berlin Heidelberg New York, pp 279–295

Détraz G (1984) Étude géologique du bord interne de la zone Houillère briançonnaise entre la vallée de l’Arc et le massif de Péclet-Polset (Alpes de Savoie). PhD Thesis, University of Grenoble

Eteradossi O (1983) Les roches vertes orthodérivées du massif du Ruitor (Alpes franco-italiennes): pétrographie et géochimie. DEA, University of Grenoble

Evensen NM, Hamilton PJ, O’Nions RK (1978) Rare-earth abundances in chondritic meteorites. Geochim Cosmochim Acta 42:1199–1212

Fabre J (1961) Contribution à l’étude de la zone houillère en Maurienne et en Tarentaise (Alpes de Savoie). Mém Bur Rech Géol Min 2

Fabre J, Schade J, Baudin T, Desmons J, Mercier D, Peruccio-Parison MD (1987) Relics of pre-Mesozoic events in the Briançon zone (Northern French Alps). In: Flügel HW, Sassi FP, Grecula P (eds) Pre-Variscan and Variscan events in the Alpine-Mediterranean mountain belts. Alfa Publishers Bratislava, pp 183–208

Giorgis D, Thélin P, Stampfli G, Bussy F (1999) The Mont-Mort metapelites: Variscan metamorphism and geodynamic context (Briançonnais basement, Western Alps, Switzerland). Schweiz Mineral Petrogr Mitt 79:381–398

Gouffon Y (1993) Géologie de la nappe du Grand St-Bernard entre la Doire Baltée et la frontière suisse (Vallée d’Aoste – Italie). Mém Géol Lausanne 12:1–147

Gouffon Y, Burri M (1997) Les nappes des Pontis, de Siviez-Mischabel et du Mont Fort dans les vallées de Bagnes, d’Entremont (Valais, Suisse) et d’Aoste (Italie). Eclog Geol Helv 90:29–41

Guillot F (1987) Géologie de l’Antépermien de Vanoise septentrionale (zone briançonnaise interne, Alpes occidentales, Savoie, France). PhD Thesis, University of Lille

Guillot F, Liégeois JP, Fabre J (1991) Des granophyres du Cambrien terminal dans le Mont Pourri (Vanoise, zone briançonnaise): première datation U–Pb sur zircon d’un socle des zones internes des Alpes françaises. CR Acad Sci II 313: 239–244

Guillot F, Desmons J, Ploquin A (1993) Lithostratigraphy and geochemical composition of the Mont Pourri volcanic basement, Middle Penninic W-Alpine zone, France. Schweiz Mineral Petrogr Mitt 73:319–334

Ludwig KR (1999) User’s manual for Isoplot/Ex version 2.10. Berkeley Geochron Center Spec Publ 1a, Berkeley, California

Mercier D, Baudin T (1990) Chevauchement alpin précoce du cristallin du Ruitor sur la Zone Houillère Briançonnaise (Savoie, Val d’Aoste). Soc Géol Fr (eds) 13ème Réun Sci Terre Grenoble, abstract, p 90

Paquette JL, Ménot RP, Peucat JJ (1989) REE, Sm–Nd and U–Pb zircon study of eclogites from the Alpine External Massifs (Western Alps): evidence for crustal contamination. Earth Planet Sci Lett 96:181–198

Pearce JA, Harris NBW, Tindle AG (1984) Trace element discrimination diagrams for the tectonic interpretation of granitic rocks. J Petrol 25:956–983

Pin C, Marini F (1993) Early Ordovician continental break-up in Variscan Europe: Nd–Sr isotope and trace element evidence for bimodal igneous associations of the Southern Massif Central, France. Lithos 29:177–196

Platt JP, Lister GS, Cunningham P, Weston P, Peel F, Baudin T, Dondey H (1989) Thrusting and backthrusting in the Briançonnais domain of the Western Alps. Geol Soc Lond Spec Publ 45:135–152

Pupin JP (1980) Zircon and granite petrology. Contrib Mineral Petrol 73:207–220

Saliot P (1973) Le Métamorphisme dans les Alpes françaises. PhD Thesis, Univ Paris-Orsay

Schaltegger U, Gebauer D (1999) Pre-Alpine geochronology of the Central, Western and Southern Alps. Schweiz Mineral Petrogr Mitt 79:79–87

Schuhmacher M, De Chambost E, McKeegan KD, Harrison TM, Migeon H (1994) In situ dating of zircon with the Cameca IMS-1270. In: Benninghoven A et al. (eds) Secondary ion mass spectrometry, SIMS IX. Wiley, New York, pp 919–922

Stacey JS, Kramers JD (1975) Approximation of terrestrial lead isotope evolution by a two-stage model. Earth Planet Sci Lett 26:207–221

Stampfli GM (1990) Tethyan oceans. Geol Soc Lond Spec Publ 173:1–23

Stampfli GM (1996) The Intra-Alpine terrane: a Paleotethyan remnant of the Alpine Variscides. Eclog Geol Helv 89:13–42

Stille P, Tatsumoto M (1985) Precambrian tholeiitic–dacitic rock suites and Cambrian ultramafic rocks in the Pennine nappe system of the Alps: evidence from Sm–Nd isotopes and rare earth elements. Contrib Mineral Petrol 89:184–192

Thélin P (1983) Les gneiss œillés de la Nappe du Grand Saint-Bernard, essai d'évaluation des critères susceptibles d'en préciser l'hérédité pré-métamorphique (Alpes valaisannes, Suisse). PhD Thesis, University of Lausanne

Valverde-Vaquero P, Dunning GR (2000) New U–Pb ages for Early Ordovician magmatism in central Spain. J Geol Soc Lond 157:15–26

von Raumer JF (1998) The Paleozoic evolution in the Alps: from Gondwana to Pangea. Geol Rundsch 87:407–435

von Raumer JF, Stampfli GM, Borel G, Bussy F (2002) Organization of pre-Variscan basement areas at the north-Gondwanan margin. Int J Earth Sci 91:35–52

Wiedenbeck M, Allé P, Corfu F, Griffin WL, Meier M, Oberli F, von Quadt A, Roddick JC, Spiegel W (1995) Three natural zircon standards for U–Th–Pb–Lu–Hf, trace elements and REE analyses. Geostand Newsl 19:1–23

Ziegler PA (1990) Geological atlas of Western and Central Europe. Shell International Petroleum, The Hague